Expert Systems with Applications: X 2 (2019) 100006

Contents lists available at ScienceDirect

Expert Systems with Applications: X

journal homepage: www.elsevier.com/locate/eswax

International roughness index prediction based on multigranularity fuzzy time series and particle swarm optimization

Wei Li[a], Ju Huyan[b,*], Liyang Xiao[a,*], Susan Tighe[b], Lili Pei[a]

[a] School of Information Engineering, Chang'An University, Xi'an, Shaanxi 710064, People's Republic of China
[b] Centre for Pavement and Transportation Technology (CPATT), Department of Civil and Environmental Engineering, University of Waterloo, Waterloo, Ontario, Canada, N2L 3G1

ARTICLE INFO

Article history:
Received 29 January 2019
Revised 22 May 2019
Accepted 23 May 2019
Available online 24 May 2019

Keywords:
International roughness index
Fuzzy time series
Multigranularity
Automatic clustering
Particle swarm optimization

ABSTRACT

The effective prediction of pavement performance trends can help in achieving the cost-effective management of pavements over their service life. The international roughness index (IRI) is a widely used pavement performance index, which can be considered as a time-dependent variable in terms of scientific modeling. This research aims to develop an innovative IRI prediction model based on fuzzy-trend time-series forecasting and particle swarm optimization (PSO) techniques. Raw datasets extracted from the Long-Term Pavement Performance database are used for model training, testing, and performance assessment. First, IRI values are divided into different granular spaces, which are considered as the principal factor and subfactors. In addition, the multifactor interval division method is proposed according to the principle of the automatic clustering technique. Next, a second-order fuzzy-trend model and fuzzy-trend relationship classification method are proposed to predict the fuzzy-trend of each factor. Then, the fuzzy-trend states for multiple granular spaces are generated while giving full consideration to various uncertainties. Finally, the PSO technique is used to optimize the performance model while carrying out future IRI forecasting. Comparative experiments are performed using more than 20,000 data items from different regions to verify the effectiveness of the proposed method. The experimental results indicate that the proposed method outperforms other approaches including the polynomial fitting, autoregressive integrated moving average, and backpropagation neural network methods in terms of the root mean squared error (0.191) and relative error (6.37%).

1. Introduction

In transportation engineering, the topmost consideration should be safety. Therefore, professional scientific effort should be made by both private and public sectors to comprehensively interpret service conditions and the changing mechanism of road roughness levels. The international roughness index (IRI) was initially proposed in a research project conducted by the University of Michigan (Cebon, 1993) for monitoring the overall roughness condition of certain pavements. The IRI mainly measures the longitudinal profile condition of a travelled roadway according to the vehicle vibration condition. The most widely used units for measuring the IRI are meter per kilometer and inch per mile (Zhou, Wang, & Lu, 2008).

Over the past few decades, scholars across the world have made significant effort to study the changing IRI mechanisms, which have been then used to analyze pavement performance deterioration trends (Kargah-Ostadi, Stoffels, & Tabatabaee, 2010; Lu & Tolliver, 2012; Peshkin, Hoerner, & Zimmerman, 2004; Shirazi, Ayres, Speir, Song, & Hall, 2010; Zimmerman & Peshkin, 2003). Rahim, Fiegel, Ghuzlan, and Khumann (2009) analyzed the IRI characteristics of cracked and seated concrete pavements and thereby provided maintenance and rehabilitation guidance for pavement management. However, they did not consider the climate conditions, which have significant influence on the roughness progression, especially for hot-mix asphalt overlay pavements (Perera & Kohn, 2001). Albuquerque and Núñez (2011) investigated the roughness condition of low-volume roads using multiple regression analysis. Zhao and Guo (2013) predicted the IRI over time using Markov analysis, thus providing a probabilistic IRI prediction

* Corresponding authors.
E-mail addresses: grandy@chd.edu.cn (W. Li), jhuyan@uwaterloo.ca (J. Huyan), liyang_xiao@163.com (L. Xiao), sltighe@uwaterloo.ca (S. Tighe), 2543487651@qq.com (L. Pei).

https://doi.org/10.1016/j.eswax.2019.100006

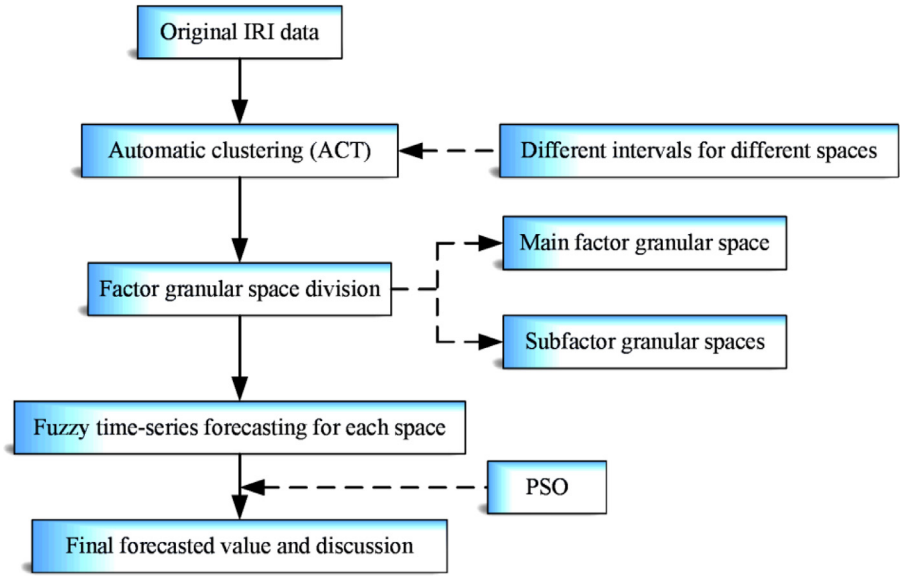

Fig. 1. Methodology framework.

method instead of a deterministic one. Qian, Jin, Zhang, Ling, and Sun (2018) proposed an exponential IRI regression model by modeling two parameters α and β and used the model to predict IRI trends over time. However, the effectiveness and robustness of the abovementioned approaches are not convincing because most regression analysis methods assume that the dataset follows certain distributions.

Typical IRI prediction models have been developed by the transportation departments of Mississippi and Washington as part of the Long-Term Pavement Performance (LTPP) program and by other state agencies based on the Mechanistic Empirical Pavement Design Guide (George, 2000; Jackson, Puccinelli, & Engineers, 2006; Officials, 2008). The development of these models is a remarkable achievement, and they are still being used for long-term pavement design and management. However, because these models are based on data-driven approaches, they still have the intrinsic drawbacks of statistic-based methods (Contreras, Espinola, Nogales, & Conejo, 2003). Thus, the performance of these models relies significantly on the quality and characteristics of the data being used. In addition, traditional approaches are influenced by the low accuracy of data acquisition, and hence, they usually fail to handle the ambiguity and uncertainty inherent in raw datasets (Reuter, 2007).

With the advancement of artificial intelligence (AI) techniques, several engineering fields are focusing on using AI approaches to facilitate research and practice tasks. In the field of pavement management, the initial attempt was made by Kargah-Ostadi et al. (2010), who proposed an intelligent method based on artificial neural networks (ANNs) to analyze the deterioration trend of pavements through IRI prediction modeling. Thereafter, researchers have used not only ANNs but also other AI techniques such as support vector machines (Abdelaziz, Abd El-Hakim, El-Badawy, & Afify, 2018; Georgiou, Plati, & Loizos, 2018) to investigate pavement roughness progression. However, these methods consider the IRI as a dependent indicator that is influenced by several other pavement conditions, traffic loading, and environmental factors at a fixed observation time, thereby ignoring the impact of time on the IRI. Time is an invisible space variable that can have an abstract existence and can contain a comprehensive combination of all other visible, traceable, and concrete influences. Hence, this variable has a direct influence on the deterioration of pavement performance, and hence, it affects the IRI. Therefore, fuzzy time-series methods should be investigated to bridge the gaps in current literature with regard to intelligent IRI predictions. Fuzzy time-series prediction methods have been successfully applied to several fields such as stock prediction and weather prediction, and these applications serve as invaluable reference for the IRI prediction research conducted in this study.

Considering the background described above, the present study aims to develop an IRI prediction approach based on an innovative fuzzy time-series analysis. To fulfill this purpose, multifactor and multigranularity analyses are considered for time-series forecasting. First, the automatic clustering technique (ACT) is adopted to generate a series interval within each granular space, which should be defined in advance. Next, a second-order fuzzy-trend matrix (SFTM) and fuzzy-trend relationship classification (FTRC) method are proposed to predict the fuzzy-trend of each factor. Then, the fuzzy-trend states of multiple granular spaces are generated while giving full consideration to various uncertainties. Finally, the particle swarm optimization (PSO) technique is employed to forecast the optimal IRI value. Comparative experiments are performed to evaluate the effectiveness of the proposed method.

2. Methodology

After a road is opened to traffic, its roughness condition tends to vary over the service time. To outline the changing mechanism of road roughness, IRI values are regarded as fuzzy time-dependent variables. Fig. 1 illustrates the framework of the proposed fuzzy time-series clustering IRI prediction methodology. As shown in the figure, the IRI values are first divided into three granular spaces. Then, the data within each granular space are assigned to a series of intervals, with each interval having a membership degree defined by fuzzy theory. Specifically, the value of the membership degree indicates the belonging probability of the concrete IRI value to the corresponding interval. In this research, the initial intervals are obtained through an automatic clustering algorithm. Thereafter, the fuzzy sets are assigned to the divided intervals according to the subordinate relationships of these sets along with the grouping statistics. Finally, the PSO method is utilized to obtain the optimal weight vector and corresponding predicted IRI value. To provide a more interpretative understanding of the methodology, the key fundamental theories are introduced in this section.

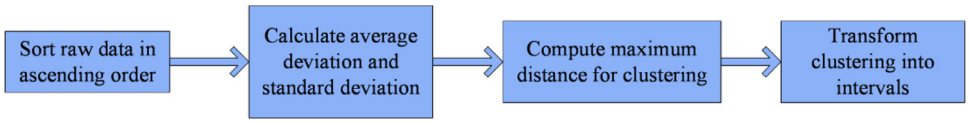

Fig. 2. ACT processes.

2.1. Fuzzy time series

In 1965, Zadeh proposed the fuzzy set theory (Sets & Zadeh, 1965; Yao, 2000), which was the theoretical foundation for fuzzy time-series analysis. On the basis of this theory, Song and Chissom (1993) developed the first fuzzy time-series model in 1993, which was a remarkable breakthrough. Later, several studies were conducted on the optimization (Chen & Jian, 2017; Chen, Manalu, Pan, & Liu, 2013; Yu, 2005) and application of time-series analysis. A few representative examples are listed here: Chen (1996) aimed to optimize the complexity of a fuzzy time-series model, Huarng (2001) proposed a heuristic algorithm (Kuo et al., 2009) to improve the accuracy of the prediction result of a fuzzy time series, and Zadeh (1996) proposed a time-series model optimized for computing with words prediction analysis.

Here, a fuzzy time series is defined as follows:

Define $U = \{u_1, u_2, \ldots, u_n\}$ as a universe of discourse. Then, a fuzzy set A of U can be represented as follows:

$$A = \frac{f_A(u_1)}{u_1} + \frac{f_A(u_2)}{u_2} + \ldots + \frac{f_A(u_n)}{u_n} \tag{1}$$

where f_A denotes the membership function of the fuzzy set A, which is mostly written in the form f_A: $U \rightarrow [0, 1]$. $f_A(u_i)$ is the membership degree of u_i within the fuzzy set A, $1 \le i \le n$.

Assume that a group of fuzzy sets $f_i(t)(i = 1, 2, \ldots)$ are defined in the universe of discourse $Y(t)(t = \ldots, 0, 1, 2, \ldots)$. $F(t)$ represents the collection of $f_i(t)(i = 1, 2, \ldots)$. Then, the collection $F(t) = \{f_1(t), f_2(t), \ldots\}$ is called a fuzzy series set in the discourse $Y(t)(t = \ldots, 0, 1, 2, \ldots)$.

Based on the above definition, the nth−order fuzzy time-series relationships for the fuzzy sets $F(t-1), F(t-2), \ldots, F(t-n)$ can be expressed as

$$F(t-n), F(t-n+1), \ldots, F(t-1) \rightarrow F(t) \tag{2}$$

Therefore, given $F(t) = A_j, F(t-1) = A_{i1}, \ldots, F(t-n) = A_{in}$, the following logical relationship can be obtained:

$$A_{in}, \ldots, A_{i2}, A_{i1} \rightarrow A_j \tag{3}$$

where $A_{in}, \ldots, A_{i2}, A_{i1}$ are called the current states, which should be known values in a certain problem. A_j is called the next state, which is to be predicted by the developed model.

2.2. Interval division using ACT

The ACT (Hao, Wang, & Tuo, 2015) is characterized by its adaptive clustering capability, which can help in minimizing the bias caused by manual parameter setting. Therefore, the ACT is adopted to generate the multiple intervals for different granular spaces. Fig. 2 illustrates the key procedures of the ACT, which are data sorting, distance calculation, automatic clustering, and interval generation.

Step 1: Sort the raw data in the ascending order, with equal values appearing only once. Then, calculate the average deviation (agv_{diff}) and standard deviation (dev_{diff}) of the sorted dataset using Eqs. (4) and (5).

$$agv_{diff} = \frac{\sum_{i=1}^{n} (d_{i+1} - d_i)}{n-1} \tag{4}$$

$$dev_{diff} = \sqrt{\frac{\sum_{i=1}^{n} (d_{i+1} - d_i - agv_{\text{diff}})^2}{n-1-1}} \tag{5}$$

where n denotes the total number of data points. $d_i (i = 1, 2, \ldots, n)$ denotes the sorted data values with $d_1 < d_2 < \ldots < d_i < \ldots < d_n$.

Step 2: Use Eq. (6) to calculate the maximum distance:

$$\max\_distance = c \times dev_{diff} \tag{6}$$

where c is a constant weight value. Here, $c = 0.5$.

Step 3: Cluster the ascending data following the calculations of Steps 1 and 2. Let d_1 be the current cluster and judge whether the next data point belongs to this current cluster or not. If not, assign it to a separate cluster. That is, if $d_{i+1} - d_i \le$ max_distance, then assign d_{i+1} to the current cluster. Otherwise, create a new cluster for d_{i+1}. Repeat the operations until all the data points are assigned to specific clusters. The clustered results can be expressed as follows:

$$\{d_{11}, \ldots d_{1a}\}, \{d_{21}, \ldots d_{2b}\}, \ldots \{d_{i1}, \ldots d_{in}\}, \ldots \left\{d_{j1}, \ldots d_{jm}\right\}$$

Step 4: Convert the clustering results to continuous intervals. Fig. 3 presents the process of converting clusters to intervals. The detailed steps are as follows. First, convert the first cluster $\{d_{11}, \ldots, d_{1a}\}$ to an interval $[d_{11}, d_{1a})$. Then, make the following two judgements: (1) Judge whether the current interval is $[d_i, d_j)$ with the current class of $\{d_k, d_l\}$. If $d_j \ge d_k$, then convert the current class $\{d_k, d_l\}$ to intervals $[d_j, d_l)$. At the same time, use $[d_j, d_l)$ as the current interval and the next cluster, which is $\{d_m, d_n\}$, as the current class. However, if $d_j < d_k$, then convert the current class $\{d_k, d_l\}$ to interval $[d_k, d_l)$ and create a new interval $[d_j, d_k)$ between $[d_i, d_j)$ and $[d_k, d_l)$. Next, use $[d_k, d_l)$ as the current interval and the next cluster, which is $\{d_m, d_n\}$, as the current class. (2) Judge whether the current interval is $[d_i, d_j)$ with the current class of $\{d_k\}$. If so, convert the current class $\{d_i, d_j\}$ to interval $[d_i, d_k)$. At the same time, use $[d_i, d_k)$ as the current interval and the next cluster, which is $\{d_m, d_n\}$, as the current class. According to this principle, process all the data points within the dataset and thus generate all the intervals.

Step 5: Calculate the medium values for all the intervals as follows:

$$mid\_value_i = \frac{low_i + upper_i}{2} \tag{7}$$

where low_i denotes the lower bound of the ith interval. Here, the superscript i denotes the upper bound of the ith interval.

2.3. Granular computing

Granular computing (GrC) is an umbrella concept and computational paradigm for information processing that simulates human thinking mechanisms. Different formalisms and information processing methodologies are included in GrC methodologies. The hierarchy structure of the computing organization mechanism of granules provides GrC with the ability to interpret complex problems from multiple perspectives. As illustrated in Fig. 4, the entire GrC structure usually includes several layers with crossed information sharing between the granules. In this figure, the deeper the layers, the finer are the unit data items, which are shown as the

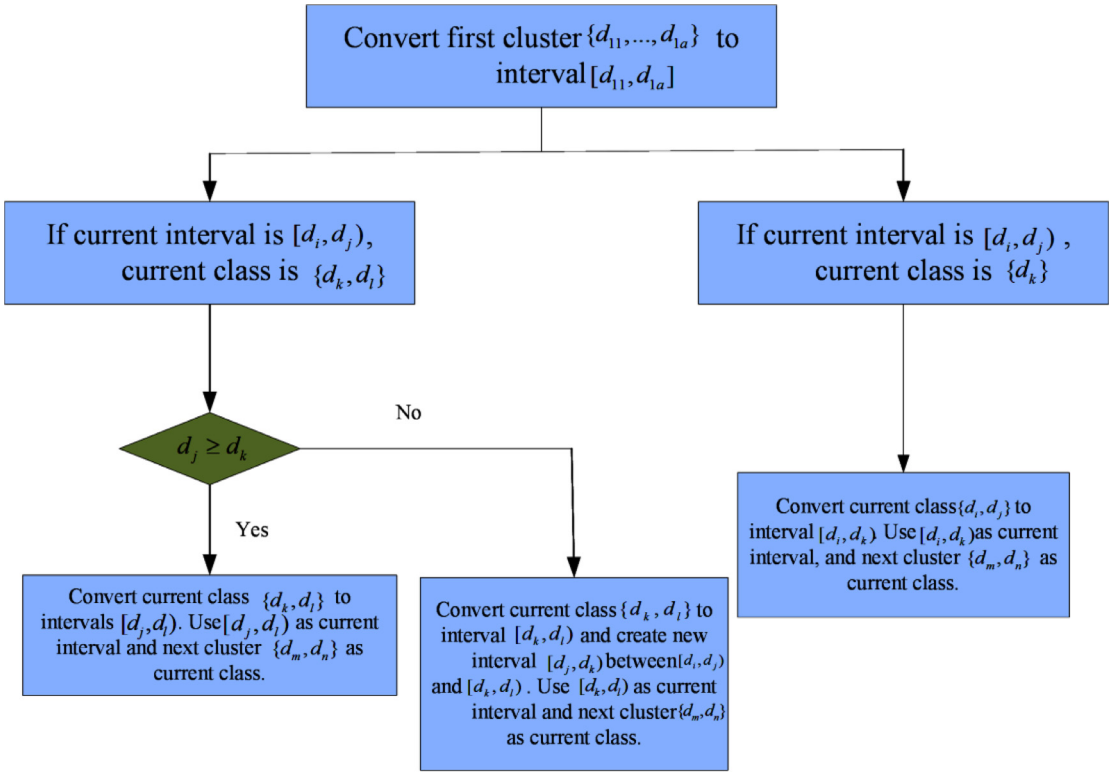

Fig. 3. Process of converting clusters to intervals.

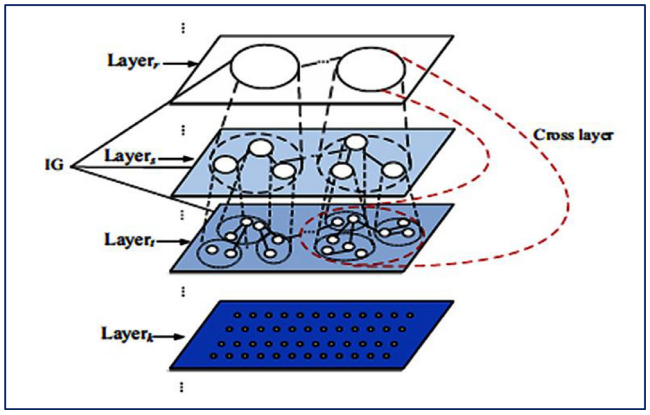

Fig. 4. Schematic of multilayer granular structure.

dots in the *k*th layer. The hierarchy property of the granular structure can be observed as well, which characterizes the novelty of GrC compared to other methods.

Generally, GrC is realized based on three basic notions: granules, granular space, and hierarchy structures (Wang, Zhang, Ma, & Yang, 2011; Yao, 2005). Granules are the unit elements of a GrC model and are distributed in their specific granular spaces. The individual granular space (father granular space) can be composed of several subgranular spaces (child granular spaces), and both the father and child granular spaces themselves can be hierarchically distributed as well. Thus, the comprehensive hierarchy of multiple granular spaces can be used to model the multifactor and multiscale organized datasets, especially for handling problems that involve both certainty and uncertainty influences that should be considered simultaneously (Chen & Tanuwijaya, 2011).

For GrC-based system development, several computing models have been proposed as a type of knowledge interpretation methodology. Popular GrC models include the fuzzy set theory, rough set theory, quotient space, and cloud model. Each of them has a specific hierarchy structure suitable for certain problems. The fuzzy set theory is mainly used for handling ambiguous data and is based on the granularity of information and if–then structures. The rough set theory is a mathematical tool for interpreting incomplete data and unveiling the hidden properties of a dataset. Hierarchy rough set structures are a typical characteristic of rough set analysis. The quotient space is characterized by quotient typology, and new space is created for the given data. The cloud model method involves forward and backward cloud transformation. Hence, the hierarchy structure of the cloud model is generated by this bidirectional transformation concept. These four typical GrC models are widely used in literature. Each has its own computing mechanism, but they share the basic ideas of GrC. In this research, the fuzzy set model is selected for IRI prediction analysis because it is more computationally efficient than the other approaches.

Specifically, each IRI measurement factor is considered as an individual granule. Therefore, three granules can be defined by three IRI factors, which are the principal factor and two subfactors. Then, we define three granular spaces: (1) the first granular space containing only the principal factor, (2) the second granular space containing the principal factor and one of the subfactors, and (3) the third granular space containing the principal factor and both the subfactors.

2.4. PSO

PSO (Hao et al., 2015) is a heuristic model optimization algorithm based on the simulation of animal movement behavior. The innovative idea behind this method is that animals are able to select the optimum speeds and directions in moving toward their desired destinations. The heuristic aspect of the PSO method is that no assumptions are required for handling the specific tasks when using this method.

The PSO algorithm is a global random search algorithm based on swarm intelligence and hence is more intelligent than traditional methods. The main idea behind this method is the simulation of the migration and clustering behavior during bird foraging. Various organisms in nature have certain group behaviors; thus, one of the main research areas of artificial life is to explore the group behaviors of natural organisms, thereby constructing intelligent models for solving practical problems with scientific perspectives.

In most situations, PSO is used to optimize the solutions of other methods instead of providing independent models. Specifically, potential solutions to a certain problem are regarded as birds, called particles, in the solution space. Each particle has a fitness value that is determined by the defined fitness function and has a velocity that determines the direction and distance from which the particle is to move toward the optimum position. When the specific optimization problem has been established, a group of random particles (random solutions) is generated to initialize the particles. Then, the moving velocity and positions of the particle are iteratively updated to find the optimal solution. In each iteration, the particle updates itself by tracking two extremums: the optimal solution found by the particle itself, which is called the individual extremum, and the optimal solution found among the entire population in the current state, which is called the global extremum. Finally, the optimized model is obtained when the satisfied fitness value is achieved.

Therefore, the primary consideration of utilizing PSO in this research is based on the three abovementioned reasons, which can be summarized as follows: (1) PSO is an intelligent algorithm that outperforms traditional methods, yet few studies have used this approach to analyze pavement roughness conditions. (2) PSO is best utilized when it is combined with other methods to solve certain optimization problems instead of being independently used for model building. In this manner, PSO can serve as an effective approach to solve complex optimization problems. (3) The PSO method has been proven to be significantly effective in solving different types of problems; hence, this research aimed to determine the effectiveness of the PSO method in solving the problem of IRI prediction.

Specifically, a particle swarm is formed by a group of particles that represent the potential solutions. Each individual particle has its initial position and moving velocity. By calculating the objective function, the particle should update its position based on the velocity toward the best position, which represents the optimum solution of a certain problem. To ensure that the final solution is optimum from a global perspective, the individual local best position (P_{best}) and global best solution (P_{gbest}) should be updated repeatedly during the model optimization process. The global best solution is updated based on the local best solution, which is obtained by revising the current position based on the velocity and direction of the particle. The velocity and position update functions for particle i are defined in Eqs. (8) and (9), respectively.

$$V_{i,k} = w \times V_{i,k-1} + C_1 \times r_1 \times \left(P_{best,i} - W_{i,k-1}\right) + C_2 \times r_2 \times \left(P_{gbest} - W_{i,k-1}\right) \tag{8}$$

$$P_{i,k} = P_{i,k-1} + V_{i,k} \tag{9}$$

where $V_{i,\,t}$ and $P_{i,\,k}$ respectively represent the velocity and position of the ith particle in the kth iteration. w denotes the inertial weight coefficient. C_1 and C_2 are the constant parameters that are decided based on the properties of a specific problem. In the present case, we set $C_1 = C_2 = 2.r_1$ and r_2 are normalization parameters having Gaussian distributions.

The procedures of the PSO optimization algorithm are based on the above definitions and explanations, as illustrated in Fig. 5.

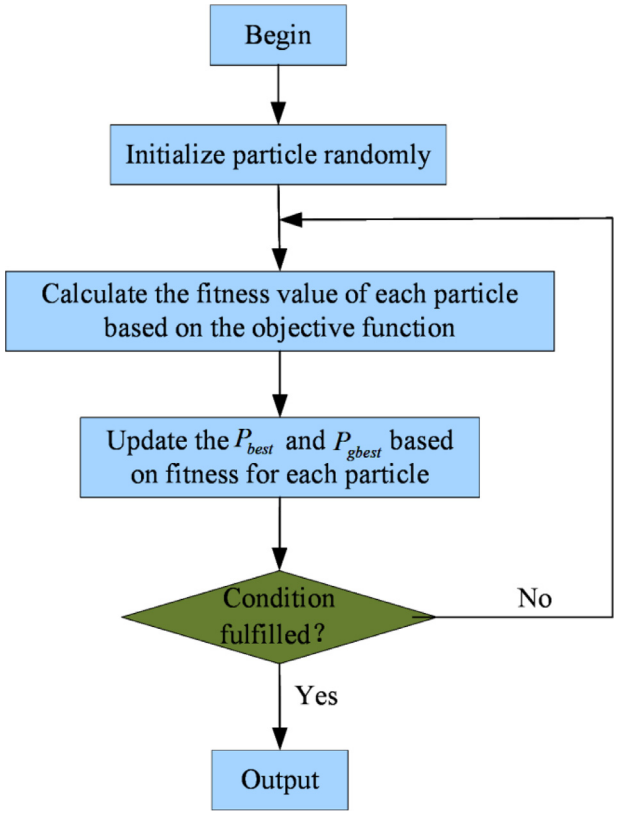

Fig. 5. PSO flowchart.

3. Multigranularity-combination-based IRI prediction

This research proposed a state-of-the-art IRI prediction model based on a fuzzy time-series forecasting methodology facilitated by multigranularity PSO. As shown in Fig. 6, the prediction process is divided into five main steps. In this section, the detailed calculations in each step are discussed.

Step 1: ACT-based interval division: Fig. 7 shows the interval division process based on the ACT. Assume that the universe of discourse of the principal factor is divided into p intervals, which are represented as $u_1, u_2, \ldots u_p$. If the jth subfactor belongs to the interval represented as m_j, then assign it to this interval. This affiliation can be represented as $v_{j,1}, v_{j,2}, \ldots, v_{j,m_j}$.

Step 2: FTRC realization: This procedure can be divided into four steps (Fig. 8): (1) define the fuzzy sets, (2) fuzzify data, (3) construct an SFTM, and (4) build FTRC for each factor. The details of these steps are as follows.

(1) Define fuzzy sets for both the principal factor and subfactors: Consider that $A_1, A_2, \ldots, A_p$ represent the fuzzy set of the principal factor and $B_{j,1}, B_{j,2}, \ldots, B_{j,mj}$ represent the fuzzy sets of the j^{th} subfactors. These two definitions are expressed in Eqs. (10) and (11).

$$\begin{aligned} A_1 &= \frac{1}{u_1} + \frac{0.5}{u_2} + \frac{0.5}{u_3} + \frac{0.5}{u_4} \ldots + \frac{0}{u_P} \\ A_2 &= \frac{0.5}{u_1} + \frac{1}{u_2} + \frac{0.5}{u_3} + \frac{0}{u_4} \ldots + \frac{0}{u_P} \\ A_3 &= \frac{0}{u_1} + \frac{0.5}{u_2} + \frac{1}{u_3} + \frac{0.5}{u_4} \ldots + \frac{0}{u_P} \\ &\ldots \quad \ldots \\ A_P &= \frac{0}{u_1} + \frac{0}{u_2} + \frac{0}{u_3} + \frac{0}{u_4} \ldots + \frac{1}{u_P} \end{aligned} \tag{10}$$

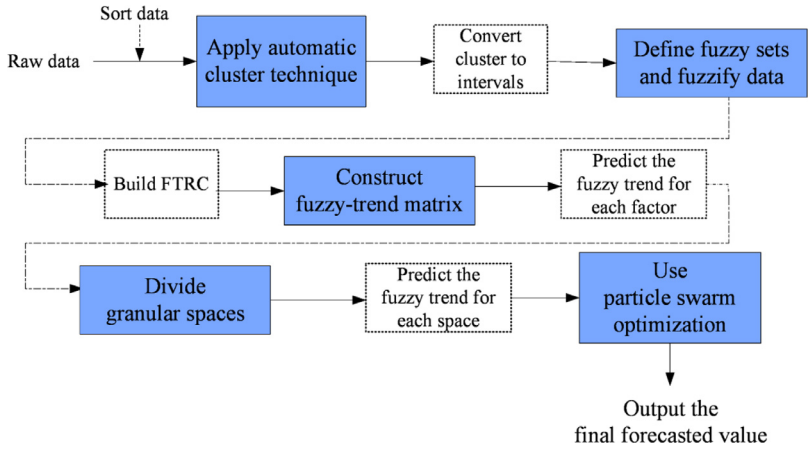

Fig. 6. Illustration of IRI prediction model.

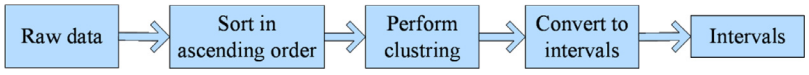

Fig. 7. Interval division by ACT.

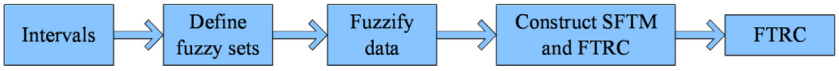

Fig. 8. FTRC realization.

$$
\begin{aligned}
B_{j,1} &= \frac{1}{v_{j,1}} + \frac{0.5}{v_{j,2}} + \frac{0.5}{v_{j,3}} + \frac{0.5}{v_{j,4}} \ldots + \frac{0}{v_{j,\ m_j}} \\
B_{j,\ 2} &= \frac{0.5}{v_{j,1}} + \frac{1}{v_{j,2}} + \frac{0.5}{v_{j,3}} + \frac{0}{v_{j,4}} \ldots + \frac{0}{v_{j,m_j}} \\
B_{j,3} &= \frac{0}{v_{j,1}} + \frac{0.5}{v_{j,2}} + \frac{1}{v_{j,3}} + \frac{0.5}{v_{j,4}} \ldots + \frac{0}{v_{j,m_j}} \\
&\ldots \quad \ldots \\
&\ldots \quad \ldots \\
B_{j,m_j} &= \frac{0}{v_{j,1}} + \frac{0}{v_{j,2}} + \frac{0}{v_{j,3}} + \frac{0}{v_{j,4}} \ldots + \frac{1}{v_{j,m_j}}
\end{aligned} \tag{11}
$$

where $u_i,\ i = 1, 2, \ldots, p$ and v_{j,m_j} denotes the intervals divided by the ACT.

(2) Fuzzify data: Based on the fuzzy sets defined previously, assign all the recorded historical data to the intervals they belong to. If a certain value is within the interval of u_i, then fuzzify that value into A_i. Similarly, if that value belongs to the interval $v_{j,\ k}$, then fuzzify it into $B_{j,\ k}$.

(3) Construct a second-order fuzzy-trend matrix (SFTM) for the fuzzified data: Assume that the fuzzy datasets of the principal factor are A_{i2}, A_{i1}, and A_m at time points $t-2,\ t-1$, and t, respectively. Then, the SFTM of the principal factor can be described as $A_{i2}, A_{i1} \rightarrow A_m$. Similarly, the SFTM of the subfactors are expressed as $B_{j,\ k2}, B_{j,\ k1} \rightarrow A_m$.

(4) Build FTRC for each factor: The fuzzy datasets at time points $t-2$ and $t-1$ are considered as the current states, whereas that at the time point t is regarded as the next state. The FTRC of the principal factor can be expressed as

$$
\begin{cases}
\text{if i2} > i1 (\text{or k2} > k1),\ classify \text{ SFTM to group 1} \\
if\ \text{i2} = \text{i1}\ (\text{ or k2} = \text{k1}),\ classify \text{ SFTM to group 2} \\
if\ \text{i2} < i1\ (\text{ or k2} < k1),\ classify \text{ SFTM to group 3}
\end{cases} \tag{12}
$$

Table 1
FTRC realization.

Classification	Relationship (i_2/k_2 and i_1/k_1)
Group 1	Descending
Group 2	Equal
Group 3	Ascending

Table 2
Fuzzy-trend matrix.

Group	Relationship					
	Descending		Equal		Ascending	
	Sum	Count	Sum	Count	Sum	Count
Group 1	$S_{d(1)}$	$N_{d(1)}$	$S_{e(1)}$	$N_{e(1)}$	$S_{a(1)}$	$N_{a(1)}$
Group 2	$S_{d(2)}$	$N_{d(2)}$	$S_{e(2)}$	$N_{e(2)}$	$S_{a(2)}$	$N_{a(2)}$
Group 3	$S_{d(3)}$	$N_{d(3)}$	$S_{e(3)}$	$N_{e(3)}$	$S_{a(3)}$	$N_{a(3)}$

Based on this equation, the FTRC can be obtained, as listed in Table 1.

Step 3: Fuzzy-trend calculation for the individual factor: Construct the fuzzy-trend matrix (Table 2), which is used to predict the fuzzy-trend for each factor. Fig. 9 illustrates the procedures of this method.

Based on the fuzzy relationships presented in Table 1, a fuzzy-trend matrix with a size of 3×6 is constructed (Table 2) and assigned to each factor. In Table 2, $S_{d(i)}$ represents the sum of the descending trends for group i, and $N_{d(i)}$ represents the total number of descending relationships. $S_{e(i)}$ represents the sum of the equal trends of all SFTMs for group i, and $N_{e(i)}$ represents the total number of equal relationships. $S_{a(i)}$ represents the sum of the ascending trends for group i, and $N_{a(i)}$ represents the total number of ascending relationships. The calculation principles are as follows.

Consider the principal factor whose SFTM is expressed as A_{i2}, $A_{i1} \rightarrow A_m$. If $i_1 > m$, then update the corresponding values based on

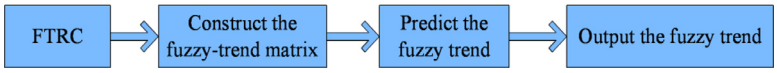

Fig. 9. Fuzzy-trend prediction process.

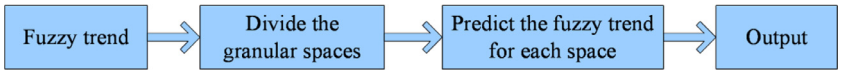

Fig. 10. Granular space division process.

Fig. 11. Final predicted value calculation.

the following equations:

$$S_{d(i)} = S_{d(i-1)} + (mid\_value_m - mid\_value_{i1}) \tag{13}$$

$$N_{d(i)} = N_{d(i-1)} + 1 \tag{14}$$

$$S_{e(i)} = 0 \tag{15}$$

$$N_{e(i)} = N_{e(i)} + 1 \tag{16}$$

Otherwise, if $i_1 < m$, then $S_{a(i)}$ and $N_{a(i)}$ should be updated according to the following equations:

$$S_{a(i)} = S_{a(i-1)} + (mid\_value_m - mid\_value_{i1}) \tag{17}$$

$$N_{a(i)} = N_{a(i-1)} + 1 \tag{18}$$

Assume that the SFTM of the current state belongs to group *i*. Then, the fuzzy-trend in the next state can be predicted by the following equation:

$$\Delta_{trend} = \frac{S_{d(i)}}{N_{d(i)}} \times \frac{N_{d(i)}}{N_{d(i)} + N_{e(i)} + N_{u(i)}} + \frac{S_{u(i)}}{N_{u(i)}} \times \frac{N_{u(i)}}{N_{d(i)} + N_{e(i)} + N_{u(i)}} \tag{19}$$

Step 4: Fuzzy-trend calculation for multigranular spaces: Divide the original dataset into $(n+1)$ granular spaces and predict the fuzzy-trend for each granular space based on the processes illustrated in Fig. 10. In this study, the first granular space is defined as the principal factor, the second granular space is composed of the principal factor and one subfactor, and the $(n+1)$th granular space is composed of the principal factor and n subfactors. Here, n denotes the number of subfactors.

In this procedure, the fuzzy-trend Δ_{m+1} and corresponding predicted value $R_{m+1}(t)$ of the $(m+1)$th granular space can be calculated using the following equations:

$$FW_M = \frac{1}{1 + \sum_{j=1,2,\ldots\ldots,m,r_j>0} r_j} \tag{20}$$

$$FW_{s(j)} = \frac{r_j}{1 + \sum_{j=1,2,\ldots\ldots,m,r_j>0} r_j} \tag{21}$$

$$\Delta_{m+1} = FW_M \times \Delta_M + \sum_{j=1}^{m} \left(FW_{s(j)} \times \Delta_{s(j)}\right) \tag{22}$$

$$R_{m+1}(t) = R(t-1) + \Delta_{m+1} \tag{23}$$

where $R(t-1)$ represents the raw data of the principal factor at the time point $t-1$, Δ_m is the predicted fuzzy-trend of the principal factor, and $\Delta_{S(j)}$ is the predicted fuzzy-trend of the jth subfactor. In addition, r_j is the correlation coefficient between two factors: (1) the average trend variation vector of the principal factor $V_M = (\frac{S_{d(i)}}{N_{d(i)}}, \frac{S_{e(i)}}{N_{e(i)}}, \frac{S_{u(i)}}{N_{u(i)}})$ and (2) the average trend variation vector of the j^{th} subfactor $V_{S(j)} = (\frac{S_{d(k)}}{N_{d(k)}}, \frac{S_{e(k)}}{N_{e(k)}}, \frac{S_{u(k)}}{N_{u(k)}})$.

Step 5: PSO-based optimum solution calculation: The optimal weight vector should be trained to calculate the final predicted result. Fig. 11 shows the detailed process.

First, the training dataset should be expressed as $T = (M, N)$ according to the following equation:

$$M = \begin{bmatrix} R_1(t-1) \ldots R_{m+1}(t-1) \ldots R_{n+1}(t-1) \\ \ldots \\ R_1(t-i) \ldots R_{m+1}(t-i) \ldots R_{n+1}(t-i) \\ \ldots \\ R_1(t-p) \ldots R_{m+1}(t-p) \ldots R_{n+1}(t-p) \end{bmatrix},$$

$$N = \begin{bmatrix} R(t-1) \\ \ldots \\ R(t-i) \\ \ldots \\ R(t-p) \end{bmatrix} \tag{24}$$

where $\boldsymbol{M}$ is a matrix formulated by the predicted values of p observations. $\boldsymbol{N}$ is the vector constructed by the corresponding ground truth values. $n+1$ denotes the total number of granular spaces. $R_{m+1}(t-i)$ and $R(t-i)$ denote the predicted values and corresponding ground truth values for the ith observation in the $(m+1)$th granular space.

Next, the optimum weight vector should be determined by the PSO method. In this procedure, q particles are generated within the $(n+1)$ granular spaces. The position of the ith particle is expressed as $W_i = \{w_{i,1}, w_{i,2}, w_{i,3}, \ldots\ldots, w_{i,n+1}\}$, which should meet the condition $w_{i,j} \in [0, 1]$ while $w_{i,1} + w_{i,2} + w_{i,3} + \ldots + w_{i,n+1} = 1$. Similarly, the velocity of the i^{th} particle is expressed as $V_i = \{v_{i,1}, v_{i,2}, v_{i,3}, \ldots\ldots, v_{i,n+1}\}$, which should meet the condition $v_{i,j} \in [-1, 1]$, $i \le j \le n+1$. Both the position and velocity of each particle are initialized with random values. In this study, the fitness function is defined as

$$f(i) = \frac{1}{n+1} \times \sum_{i} (N - M \times W_i) \tag{25}$$

where $f(i)$ denotes the fitness value with $1 \le i \le q$. Here, q represents the number of particles generated in $(n+1)$ granular spaces. $\boldsymbol{M}$ and $\boldsymbol{N}$ are defined in the same manner as that in Eq. (24). $\boldsymbol{W}_i$ denotes the position vector.

For an individual particle, after the update of each position and velocity, the corresponding fitness value should be calculated by Eq. (25). When the best fitness value is obtained, the forecasting trend and forecasted value can be calculated by Eqs. (26) and (27), respectively.

$$\Delta_z = \sum_{i=0}^{n} w_{i+1} \Delta_{i+1} \tag{26}$$

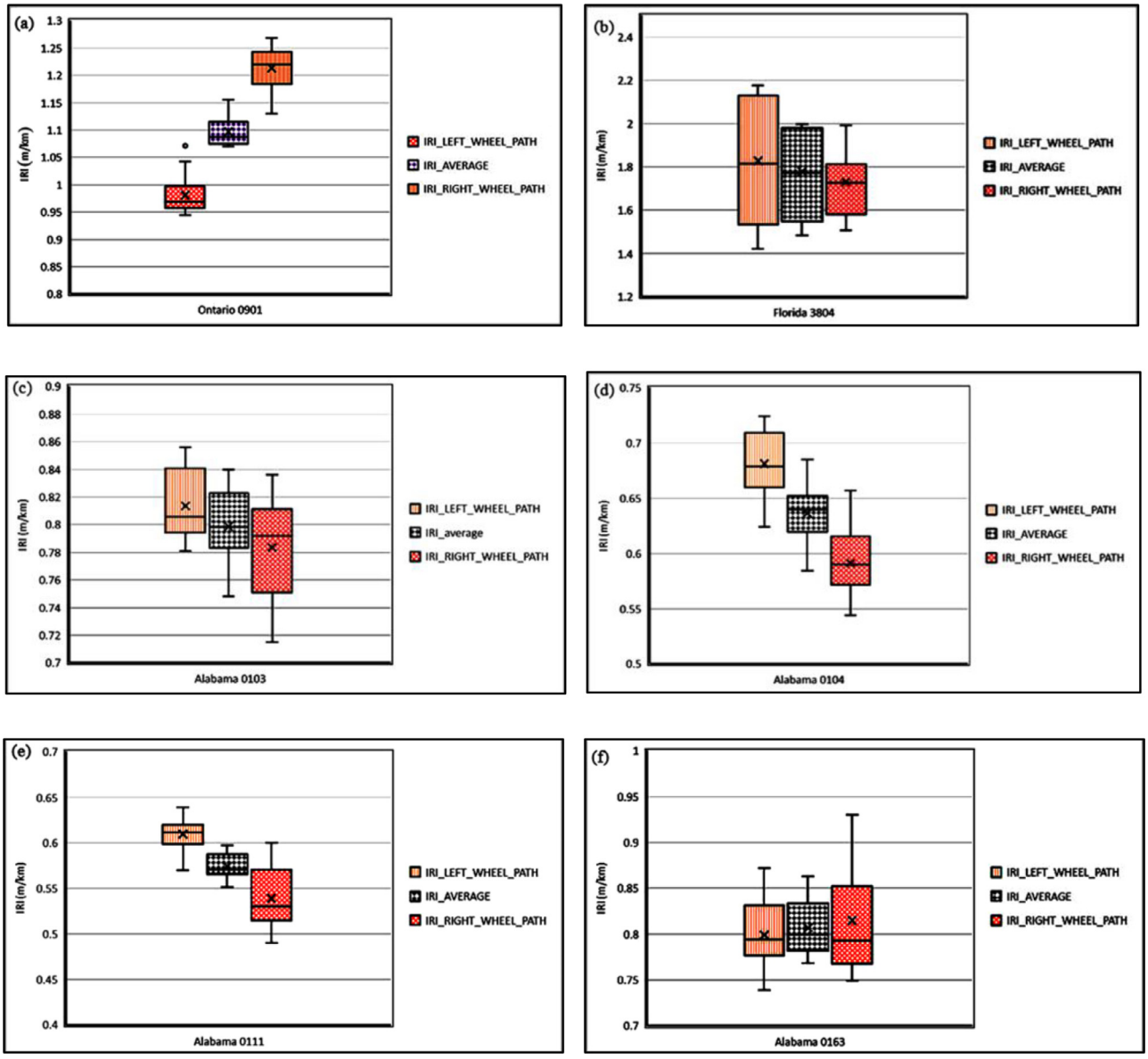

Fig. 12. Illustration of IRI distribution.

$$FR(t) = R(t-1) + \Delta_z \tag{27}$$

where Δ_{i+1} denotes the fuzzy-trend of the $(i+1)$th granular space. Δ_z denotes the corresponding forecasted fuzzy-trend. If $\Delta_z > 0$, the next state is considered to be in the ascending trend. Otherwise, it should be considered to be in the descending trend.

4. Implementation details

4.1. IRI data extraction and analysis

IRI prediction experiments are performed using the proposed multigranularity fuzzy time-series method. Original IRI data are extracted from the LTPP database. Different from the traditional methods, which consider only a single factor when predicting IRI changes, the proposed method utilizes multiple factors. Specifically, the average IRI values are selected as the principal factor, and the IRIs measured in the left and right wheel paths are used as the subfactors. The model predicts the average IRI in the next state with comprehensive consideration of the IRI values in the current state. Therefore, the results are more reliable.

Two significant phenomena are observed in the raw dataset:

(1) The IRI distributions in different regions at the same time are significantly different from each other. This phenomenon can be seen in Fig. 12. By comparing parts (a), (b), and (c) of this figure, it can be concluded that the global geographic locations (regions) of the pavements have significant influence on the IRI values. Fig. 12(c)–(f) indicate that IRI variance still exists between different road sections within the same global geographic location (region). However, the IRI difference between regions is more significant than that between the different sections of the same region.

(2) If no maintenance work is being carried out, the IRI tends to increase with the service time. This phenomenon can be seen in Fig. 13, where parts (a), (b), and (c) represent the road sections that have not undergone maintenance operations, according to the LTPP database. It is found that the overall trends of IRI changes agree with the expected increasing phenomenon, and only minor fluctuations are observed in section Alabama 0103 (Fig. 13(b)), which can be attributed to the errors introduced during data collection. Two

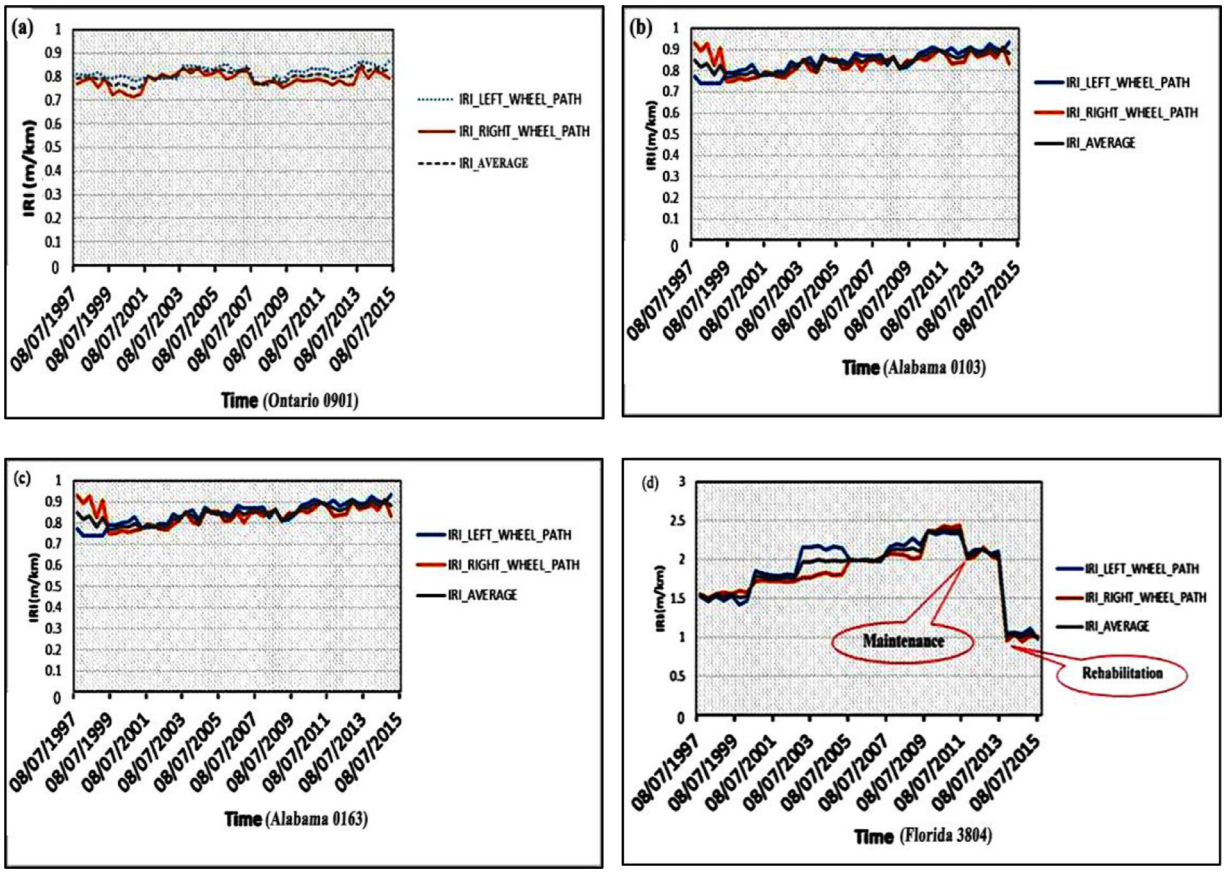

Fig. 13. IRI changes with time.

Table 3
Results of interval division.

Factor	Intervals
Principal factor	[0.991, 1.216], [1.216, 2.182], [2.182, 2.268], [2.268, 2.653], [2.653, 2.682], [2.682, 2.917], [2.917, 3.075]
Subfactor 1	[0.895, 1.137], [1.137, 1.791], [1.791, 1.825], [1.825, 1.926], [1.926, 2.006], [2.006, 2.07], [2.07, 2.076], [2.076, 2.146], [2.146, 2.205]
Subfactor 2	[1.025, 1.304], [1.304, 2.561], [2.561, 2.615], [2.615, 3.207], [3.207, 3.366], [3.366, 3.732], [3.732, 3.845], [3.845, 4.027]

repairing operations have been conducted in section Florida 3804 according to the records in the database. The first operation was a minor maintenance task, which reduced the IRI from around 2.5 to 2.0. After two years, a rehabilitation was carried out, which reduced the IRI to close to 1.0. This indicates that appropriate repairing work can improve the overall performance of the pavement. Therefore, the development of effective IRI prediction models to forecast the trends in potential IRI changes is very meaningful, and these models can be used to schedule cost-effective maintenance operations.

4.2. IRI forecast experiments

Because the IRI distribution is different for different regions, this research extracts datasets from 38 provinces/states in North America (Fig. 14). Thus, more than 20,000 data items are obtained to train the model, and hence, the robustness of the method can be assured. The experiments are discussed in detail below.

(1) Interval division using ACT

First, the original data are sorted in the ascending order. The average and standard deviations of each factor are calculated. Then, intervals are generated based on the proposed ACT. Table 3 presents the generated intervals.

(2) Fuzzy set formulation and FTRC establishment

First, the fuzzy sets are formulated as follows:

$$A_1 = \frac{1}{u_1} + \frac{0.5}{u_2} + \ldots + \frac{0}{u_7}$$
$$A_1 = \frac{0.5}{u_1} + \frac{1}{u_2} + \ldots + \frac{0}{u_7}$$
$$\ldots$$
$$A_1 = \frac{0}{u_1} + \frac{0}{u_2} + \ldots + \frac{0}{u_7} \quad (28)$$

Next, FTRCs are built based on the SFTM. Table 4 presents a part of the FTRCs for different factors. According to the fuzzy-trend relationships defined in Table 1, Group 2 indicates equal trending between two adjacent intervals. Therefore, the entire data presented in Table 4 have equal trending, which indicates that the roughness conditions of these road sections have no significant variance between each other. It should be noted that no groups are assigned to the values in the first two rows of Table 4, which are indicated by a slash (/). These two values are not assigned to any groups because the group of current values is decided based on the evaluation of the two values ahead of the current values.

Fig. 14. Regions considered for dataset selection.

Table 4
Part of FTRC result.

Average IRI	Fuzzy set	Group	Left-wheel-path IRI	Fuzzy set	Group	Right-wheel-path IRI	Fuzzy set	Group
1.070999	A1	/	0.964999	B1,1	/	1.177000	B2,1	/
1.080000	A1	/	0.953999	B1,1	/	1.20599	B2,1	/
1.100999	A1	2	0.968999	B1,1	2	1.233000	B2,1	2
1.105999	A1	2	0.968999	B1,1	2	1.243000	B2,1	2
1.082999	A1	2	0.975000	B1,1	2	1.190999	B2,1	2
1.080000	A1	2	0.944000	B1,1	2	1.215999	B2,1	2
1.085999	A1	2	0.952000	B1,1	2	1.218999	B2,1	2
1.103000	A1	2	0.958000	B1,1	2	1.248999	B2,1	2
1.072000	A1	2	0.962000	B1,1	2	1.182000	B2,1	2
1.088000	A1	2	0.954999	B1,1	2	1.220999	B2,1	2
1.075999	A1	2	0.992999	B1,1	2	1.159000	B2,1	2
1.070000	A1	2	0.949000	B1,1	2	1.190999	B2,1	2

Table 5
Fuzzy-trend matrix for three factors.

(a) Principal factor

Group	Descending		Equal		Ascending	
	Sum	Count	Sum	Count	Sum	Count
1	0	0	0	1	1.375	1
2	−1.717	2	0	30	1.520	3
3	0	0	0	4	0.733	2

(b) Subfactor 1

Group	Descending		Equal		Ascending	
	Sum	Count	Sum	Count	Sum	Count
1	−0.107	1	0	1	0.996	5
2	−0.725	3	0	20	1.483	4
3	−0.623	3	0	5	0.068	1

(c) Subfactor 2

Group	Descending		Equal		Ascending	
	Sum	Count	Sum	Count	Sum	Count
1	0	0	0	0	1.029	2
2	−0.148	1	0	31	1.211	3
3	−0.323	1	0	4	0.656	1

(3) Fuzzy-trend prediction for each factor

Three fuzzy-trend matrixes are generated according to the principle used to obtain the matrix in Table 2. Accordingly, the matrixes presented in Table 5 (a)–(c) are obtained. From these results, it can be inferred that few IRI values show descending trends, i.e., negative values. Most values remain constant, which is indicated by the number 0. However, the IRI values for some road sections show ascending trends. These phenomena indicate that the roughness changing mechanisms in different road sections are significantly different even though they are distributed within limited ranges.

Thereafter, the fuzzy-trends of these three factors are calculated using Eq. (19). Here, the calculated fuzzy-trends are $\Delta_{principal} = 0.688$, $\Delta_{subfactor1} = 0.127$, $\Delta_{subfactor2} = 0.030$. These results indicate that all the fuzzy-trends tend to increase with time because all of them are above 0.

(4) Fuzzy-trend forecast

The fuzzy-trends are constructed in multiple granular spaces. As discussed before, the first granular space includes only the average IRI values, the second granular space includes the average IRIs and one of the wheel-path IRIs, and the third granular space includes all the IRIs. Then, the fuzzy-trends and values of these granular spaces can be calculated using Eqs. (20)–(23).

$$\Delta 1 = 0.688,\ \Delta 2 = 0.4145,\ \Delta 3 = 0.248$$

$$R1(t) = 3.684,\ R2(t) = 3.411,\ R3(t) = 3.244$$

(5) Calculation of optimal weight vector based on PSO

In this study, 25 particles are used for model optimization. The optimum results are obtained after 200 iterations of parameter updating. Then, according to Eqs. (8) and (9), the optimal weighting vector is calculated as $w = (0.26,\ 0.11,\ 0.63)$. Finally, the predicted IRI value is obtained based on Eqs. (26) and (27). The calcu-

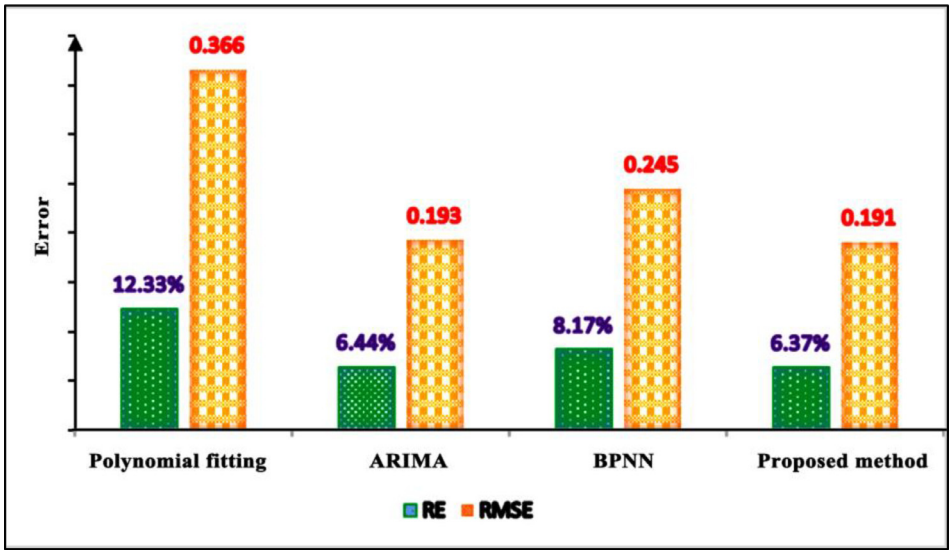

Fig. 15. Performance of different methods.

lated values obtained from the experiment are

$$\Delta_z = 0.26 \times 0.6875 + 0.11 \times 0.4145 + 0.63 \times 0.2477 = 0.3804$$

$$FR(\mathrm{t}) = 2.996 + 0.3804 = 3.3764$$

Here, the calculated Δ_z is higher than 0, which indicates that the IRI tends to increase in the next state. *FR*, which is the forecasted IRI value in the next state, is 3.3764.

5. Results

To further verify the effectiveness of the proposed method, comparative experiments are performed. The polynomial fitting, autoregressive integrated moving average (ARIMA), and backpropagation neural network (BPNN) methods are selected for IRI prediction, and the errors of these methods are compared with the results of the proposed method.

Two error indexes—the root mean squared error (RMSE) and relative error (RE)—are used to evaluate the feasibility of each method. These two indexes are calculated as follows:

$$\mathrm{RMSE} = \sqrt{\frac{\sum_{i=1}^{N} (p_i - gt_i)^2}{N}} \tag{29}$$

$$RE = \frac{|p_i - gt_i|}{gt_i} \times 100\%, \ i = 1, 2, \ldots, N \tag{30}$$

where N denotes the number of the dataset. p_t and gt_t denote the i^{th} predicted IRI value and ground truth IRI value, respectively.

As indicated by the error distributions shown in Fig. 15, the proposed method achieved the smallest error indexes (RE = 6.37%, $RMSE$ = 0.191), followed by the ARIMA method (RE = 6.44%, $RMSE$ = 0.193). The polynomial fitting method has the least performance, which might be caused by the fact that traditional fitting methods are less capable of extracting comprehensive information from big datasets.

6. Discussion

In this research, IRI data for 19 years (1997–2015) are extracted from the LTPP database for modeling. The IRI values were collected by the Federal Highway Administration. We select the IRI values for the pavement section Ontario 0901, Canada, to illustrate the entire prediction process. In addition, the IRI values for the pavement sections Florida 3804, Alabama 0103, and Alabama 0163 are extracted to perform comparative experiments.

Because times-series prediction relies highly on historical data, the data from 1997 to 2014 are collected for model training. Then, the trained model is used to predict the IRI value for the year 2015. The IRI values extracted from the LTPP database are considered as ground truth values to calculate the errors of the model. Thus, the IRI values used for model training are considered as the current state, whereas the IRIs for the year 2015 (the last year) are regarded as the next state to be predicted.

Moreover, the prediction performance of the proposed method is compared with those of other widely used methods to verify the effectiveness and reliability of the proposed method. In summary, the following conclusions can be drawn from this research:

(1) The original IRI data are divided into different length of intervals using the ACT. Then, three 3 × 6 fuzzy-trend matrixes are constructed to forecast the fuzzy-trend for each IRI factor. The forecasting is achieved by defining the fuzzy sets and establishing FTRC.
(2) To handle the uncertainty and achieve higher predicting accuracy, IRI factors are divided into three granular spaces. On this basis, the IRI predictions are performed within each granular space. The optimal forecasted IRI values are calculated through PSO.
(3) The proposed model employs the multigranularity method to provide highly reliable IRI predictions. By comparing the IRI prediction errors of the proposed method with those of the polynomial fitting, ARIMA, and BPNN methods, it is found that the proposed method has the smallest $RMSE$(0.191) and RE(6.37%) values, which indicate the effectiveness of the proposed approach.
(4) The experimental results demonstrate that the proposed model can not only achieve the highest accuracy in IRI prediction but also provide detailed interpretative explanations of the trends in IRI changes (ascending, equal, or descending). These advantages are expected to provide significant benefits for protective pavement maintenance management.

Data availability statement

The raw dataset used in this research can be downloaded from the LTPP InfoPave website, which can be accessed through the following link: https://infopave.fhwa.dot.gov/.

Funding

This research is funded by Natural Science Foundation of Shaanxi Province [Grant number: 2017zdjc-23], Fundamental Research Funds for the Central Universities, Chang'An University [Grant number: 300102249301, 300102249306], China.

CRediT authorship contribution statement

Wei Li: Conceptualization, Methodology, Validation, Formal analysis, Writing - original draft, Writing - review & editing, Funding acquisition. **Ju Huyan:** Conceptualization, Methodology, Validation, Formal analysis, Data curation, Writing - original draft, Writing - review & editing. **Liyang Xiao:** Methodology, Validation, Formal analysis, Data curation, Writing - original draft, Writing - review & editing. **Susan Tighe:** Validation, Formal analysis, Writing - review & editing, Funding acquisition. **Lili Pei:** Validation, Formal analysis, Data curation, Writing - review & editing.

Acknowledgements

Meanwhile, the authors would like to express sincere appreciations to the LTPP staff for maintaining the Website and making the data so readily available. Moreover, the authors would like to thank the anonymous reviewers for providing their invaluable comments.

Conflicts of interest

The authors declare no conflict of interest.

References

Abdelaziz, N., Abd El-Hakim, R. T., El-Badawy, S. M., & Afify, H. A. (2018). International roughness index prediction model for flexible pavements. *International Journal of Pavement Engineering*, 1–12. doi:10.1080/10298436.2018.1441414.

Albuquerque, F., & Núñez, W. (2011). Development of roughness prediction models for low-volume road networks in Northeast Brazil. *Transportation Research Record: Journal of the Transportation Research Board, 2205*, 198–205.

Cebon, D. (1993). *Interaction between heavy vehicles and roads* SAE Technical Paper. doi:10.4271/930001.

Chen, S.-M. (1996). Forecasting Enrollments Based on Fuzzy Time Series. *Fuzzy Sets and Systems, 81*(3), 311–319.

Chen, S.-M., & Jian, W.-S. (2017). Fuzzy forecasting based on two-factors second-order fuzzy-trend logical relationship groups, similarity measures and Pso techniques. *Information Sciences, 391*, 65–79.

Chen, S.-M., Manalu, G. M. T., Pan, J.-S., & Liu, H.-C. (2013). Fuzzy forecasting based on two-factors second-order fuzzy-trend logical relationship groups and particle swarm optimization techniques. *IEEE Transactions on Cybernetics, 43*(3), 1102–1117.

Chen, S.-M., & Tanuwijaya, K. (2011). Fuzzy forecasting based on high-order fuzzy logical relationships and automatic clustering techniques. *Expert Systems with Applications, 38*(12), 15425–15437.

Contreras, J., Espinola, R., Nogales, F. J., & Conejo, A. J. (2003). Arima models to predict next-day electricity prices. *IEEE Transactions on Power Systems, 18*(3), 1014–1020.

George, K. (2000). *Mdot pavement management system: prediction models and feedback system*. Mississippi: Dept. of Transportation.

Georgiou, P., Plati, C., & Loizos, A. (2018). Soft computing models to predict pavement roughness: A comparative study. *Advances in Civil Engineering, 2018*, 1–8.

Hao, C., Wang, Y., & Tuo, J. (2015). A novel particle swarm optimization algorithm with intelligent weighting mechanism. In *Information science and control engineering (ICISCE), 2015 2nd international conference on* (pp. 45–49). IEEE.

Huarng, K. (2001). Effective lengths of intervals to improve forecasting in fuzzy time series. *Fuzzy Sets and Systems, 123*(3), 387–394.

Jackson, N., Puccinelli, J., & Engineers, N. C. (2006). Long-term pavement performance program (Ltpp) data analysis support: National pooled fund study Tpf-5 (013). *Effects of multiple freeze cycles and deep frost penetration on pavement performance and cost*. Turner-Fairbank Highway Research Center.

Kargah-Ostadi, N., Stoffels, S., & Tabatabaee, N. (2010). Network-level pavement roughness prediction model for rehabilitation recommendations. *Transportation Research Record: Journal of the Transportation Research Board, 2155*, 124–133.

Kuo, I.-H., Horng, S.-J., Kao, T.-W., Lin, T.-L., Lee, C.-L., & Pan, Y. (2009). An improved method for forecasting enrollments based on fuzzy time series and particle swarm optimization. *Expert Systems with Applications, 36*(3), 6108–6117.

Lu, P., & Tolliver, D. (2012). Pavement pre-and post-treatment performance models using Ltpp data. *Journal of the Transportation Research Forum, 51*(3), 67–81 Citeseer.

Officials, T. (2008). *Mechanistic-empirical pavement design guide: A manual of practice*. AASHTO.

Perera, R., & Kohn, S. D. (2001). *Ltpp data analysis: factors affecting pavement smoothness*. Transportation Research Board, National Research Council.

Peshkin, D. G., Hoerner, T. E., & Zimmerman, K. A. (2004). *Optimal timing of pavement preventive maintenance treatment applications*. Transportation Research Board.

Qian, J., Jin, C., Zhang, J., Ling, J., & Sun, C. (2018). International roughness index prediction model for thin hot mix asphalt overlay treatment of flexible pavements. *Transportation Research Record* 0361198118768522.

Rahim, A. M., Fiegel, G., Ghuzlan, K., & Khumann, D. (2009). Evaluation of international roughness index for asphalt overlays placed over cracked and seated concrete pavements. *International Journal of Pavement Engineering, 10*(3), 201–207.

Reuter, U. (2007). *Uncertainty forecasting in engineering*. Springer.

Sets, F., & Zadeh, L. (1965). Inform. *Control, 8*, 338–353.

Shirazi, H., Ayres, M., Speir, R., Song, W., & Hall, G. (2010). Confidence level and efficient sampling size of roughness measurements for pavement management in Maryland. *Transportation Research Record: Journal of the Transportation Research Board, 2153*, 114–120.

Song, Q., & Chissom, B. S. (1993). Fuzzy time series and its models. Fuzzy Sets and Systems, *54*(3), 269–277.

Wang, G.-Y., Zhang, Q.-H., Ma, X.-A., & Yang, Q.-S. (2011). Granular computing models for knowledge uncertainty. *Journal of Software, 22*(4), 676–694.

Yao, Y. (2000). Granular computing: basic issues and possible solutions. In *Proceedings of the 5th joint conference on information sciences* (pp. 186–189).

Yao, Y. (2005). Perspectives of granular computing. *GrC, 5*, 85–90.

Yu, H.-K. (2005). A refined fuzzy time-series model for forecasting. *Physica A: Statistical Mechanics and its Applications, 346*(3-4), 657–681.

Zadeh, L. A. (1996). Fuzzy logic = computing with words. *IEEE Transactions on Fuzzy Systems, 4*(2), 103–111.

Zhao, Z., & Guo, Z. (2013). Prediction of asphalt pavement international roughness index (Iri) by combined approach of empirical regression and Markov. In *Icte 2013: Safety, speediness, intelligence, low-carbon, innovation* (pp. 2106–2113).

Zhou, G., Wang, L., & Lu, Y. (2008)., International roughness index model enhancement for flexible pavement design using Ltpp data.

Zimmerman, K., & Peshkin, D. (2003). Pavement management perspective on integrating preventive maintenance into a pavement management system. *Transportation Research Record: Journal of the Transportation Research Board, 1827*, 3–9.